Large Magnetization and Reversible Magnetocaloric Effect at the Second-Order Magnetic Transition in Heusler Materials

Large magnetization and reversible magnetocaloric effect at the second-order magnetic transition in Heusler materials

Sanjay Singh*[1], Luana Caron†[1], Sunil Wilfred D'Souza[1], Tina Fichtner[1], Giacomo Porcari[2], Simone Fabbrici[3], Chandra Shekhar[1], Stanislav Chadov[1], Massimo Solzi[2], and Claudia Felser[1]

[1]Max Planck Institute for Chemical Physics of Solids, Nöthnitzer Str. 40, 01187 Dresden, Germany
[2]Department of Physics and Earth Sciences, Parma University, Viale G.P. Usberti n.7/A (Parco Area delle Scienze) 43124 - Parma, Italy
[3]IMEM-CNR, Parco Area delle Scienze 37/A, 43124 - Parma, Italy

August 25, 2015

Magnetic materials exhibiting a large magnetocaloric effect (MCE) have recently gained strong interest due to their potential use in magnetic refrigeration technology. The MCE is intrinsic to all magnetic materials, being particularly high in the vicinity of 1^{st}- or 2^{nd}-order magnetic phase transitions [1, 2, 3, 4, 5, 6, 7, 8, 9]. Since the observation of the so-called giant MCE around room temperature in $Gd_5Ge_2Si_2$ [1], materials showing 1^{st}-order magnetic phase transitions have been investigated intensively aiming at cooling applications. However, the practical application of giant MCE materials is necessarily hindered by the nature of the phase transition itself. To induce a 1^{st}-order transition energy must be spent to overcome the potential barrier between the two phases. This leads to intrinsic irreversibilities in both entropy and adiabatic temperature changes which can drastically reduce cooling efficiency [8]. Moreover, in the case of strong 1^{st}-order phase transitions, where the crystal lattice discontinuity is the result of a symmetry change, it often results in physical instability upon thermomagnetic cycling [10].

In contrast, 2^{nd}-order magnetic transitions are continuous, which typically results into lower but fully reversible entropy changes. For instance, Gd, which has been used as a benchmark material in magnetic refrigerator prototypes [11, 12], shows a 2^{nd}-order ferro-to-paramagnetic transition close to room temperature ($T_C = 294$ K). Gd exhibits considerably high entropy change due to a

*Sanjay.Singh@cpfs.mpg.de
†Luana.Caron@cpfs.mpg.de

large magnetic moment produced by $4f$ electrons ($M_S \approx 7.5\,\mu_B$/atom). However, the high cost of Gd prohibits its use in commercial applications [13]. In contrast to rare-earth based materials, much cheaper and more environmentally friendly candidates for cooling applications were found within the family of Ni-Mn based Heusler alloys. Initial interest in this group of materials was focused in the presence of magneto-structural 1st-order martensite-austenite transitions, leading to extremely large anisotropy, entropy and adiabatic temperature changes [6, 7, 8, 9, 14, 15]. However, the martensitic phase transition is crossed at a high energy cost which translates into large hysteresis losses and low efficiency for cooling applications. It is necessary to drastically reduce thermal hysteresis to make real use of these materials.

Alternatively, in the present study we show how the flexibility of the Heusler family, can be used to optimize reversible 2nd-order magnetic phase transitions for magnetocaloric applications.

In order to maximize the energy capacity of the magnetic degrees of freedom, we need first of all to maximize the magnetization. The highest magnetization values in Heuslers are exhibited by the well-known Co-rich materials, e.g. Co_2FeSi (6 μ_B/f.u.) or Co_2MnSi (5 μ_B/f.u.) half-metals in the $L2_1$ structure (see Fig. 1 a) [16, 17, 18, 19, 20, 21, 22, 23]. On the other hand, their Curie temperatures are way too high ($\sim 10^3$ K) to make these systems useful in room temperature applications. The reason for this is the strong Co–Fe (or Co–Mn) nearest-neighbor parallel magnetic exchange coupling (Fig. 1 b). At the same time, the exchange coupling between Mn atoms, which provides the most significant contribution to magnetization ($3-4\,\mu_B$/atom), is much weaker. Albeit that simple substitution of Co by Mn decreases T_C towards room-temperature values, it does not lead to the desired increase in magnetization.

The problem is that these extra Mn atoms, which substitute Co in its position ($8c$ Wyckoff sites of the $L2_1$), become nearest neighbors to the original Mn in $4a$, and couple antiparallel to it, thereby decreasing the total magnetization (Fig. 1 c). To prevent the extra Mn from occupying $8c$ sites (so-called "antisite disorder"), they must be fully filled by transition metals other than Co, but later than Mn (i.e. located to the right of Mn in the periodic table; for the details of chemical ordering in Heusler compounds, see e.g. [24]). A good idea would be to use Ni instead of Co, since it has positive but substantially weaker exchange coupling to Mn (Fig. 1 d). This is supported by experimental observations confirming that the T_C's of Ni_2MnZ (Z= In, Sn, Sb) are quite close to room temperature [25]. On the other hand, their ground-state saturation magnetization ($\sim 4\,\mu_B$) [26] is still noticeably lower than that of Gd.

There is, however, a straightforward way to increase the magnetization, found inspecting the phase diagrams of the $Ni_2Mn_{1+x}Z_{1-x}$ (Z= In, Sn, Sb) series [25, 26]. If there is a deficit in the main-group element Z, the extra Mn atoms must occupy the $4b$ positions (Fig. 1 e). This may introduce antiparallel coupling between Mn($4a$) and Mn($4b$), as they are closer to each other when compared to Mn($4a$)–Mn($4a$) distances (i.e., $a/2 < a/\sqrt{2}$, a - lattice parameter). However, due to their mutual parallel coupling to Ni atoms Mn($4a$)–Ni($8c$)–Mn($4b$), which is relatively strong and high-coordinated, the system ef-

ficiently increases its magnetization with increasing x in a linear fashion [26]: $M_{\rm S}(x) \approx 2 \cdot m_{\rm Ni} + (1+x) \cdot m_{\rm Mn}$, where m denotes an atomic moment.

Surprisingly, $T_{\rm C}$ is rather insensitive to the changes in Mn/Z ratio and remains close to room temperature. This procedure is limited by $x \leq x_0 \approx 0.4$, which, however, corresponds to $M_{\rm S} \approx 6\ \mu_{\rm B}$/f.u., being already a significant magnetization value for Heusler materials. For $x > x_0$ the ferromagnetic system transforms into a martensite phase (with rather complicated monoclinic modulated structure [27]), with low ground state moment. Due to the higher stability of the austenite at elevated temperatures, the critical excess of Mn slightly varies with temperature as well: e.g. $0.33\ (T \approx 0) < x_0 < 0.5\ (T \approx T_{\rm C})$ and $0.32\ (T \approx 0) < x_0 < 0.4\ (T \approx T_{\rm C})$ for Z=Sb and In, respectively. Since we are interested in exploiting these materials at $T = T_{\rm C}$, we can consider the compositions at the upper limit of x_0, by making use of larger magnetization values. Based on the above speculations, here we will focus on studying the MCE of $Ni_2Mn_{1.4}In_{0.6}$ which exhibits a room temperature $2^{\rm nd}$-order phase transition ($T_{\rm C} \approx 315$ K) and large saturation magnetization ($\approx 6\ \mu_{\rm B}$/f.u.). In the following we describe in details the synthesis procedure of the austenite, as for this composition most of the experimental studies report the martensite groundstate.

The presently prepared $Ni_2Mn_{1.4}In_{0.6}$ sample (for the details, see Supporting Information) was found to stabilize in the cubic austenite structure in the entire temperature range (see Fig. 2). The Rietveld refinement of the room-temperature XRD pattern was performed assuming the $L2_1$ structure (space group $Fm\bar{3}m$), with chemical ordering as discussed above, i.e. with $8c$ sites occupied by Ni, $4a$ - by Mn, $4b$ - by In and excess Mn (see Fig. 2 b), which corresponds to the case in Fig. 1 e. The sample is found to be single phase, since all observed Bragg reflections could be indexed using the cubic $L2_1$ structure. The (111) and (200) reflections (blue arrows in Fig. 2) are clear evidence of $L2_1$ ordering [15]. The refined lattice parameter is 6.004 Å.

Magnetization curves as a function of temperature for different applied magnetic fields are shown in Fig. 3. As it clearly follows, no transition into a low-magnetic phase is observed within the whole temperature range $0 < T < T_{\rm C}$, which is in contrast to some earlier reports [28, 29] for close compositions, but in agreement with, e.g. [25, 26]. The magnetic ordering temperature value is about $T_{\rm C} \approx 316$ K, close to optimal for MCE applications. Thus we can conclude, that the present composition is close to the limit of structural instability, presenting the highest possible magnetization moment. The saturation magnetization value measured at 2 K is 6.13 $\mu_{\rm B}$/f.u. (see Fig. 4 a). Since no hysteresis associated with this transition is observed even at low fields (see the inset of Fig. 3) and the monotonic increase of magnetization with increasing field under isothermal conditions (see Fig. 4 b), we can conclude that the transition is $2^{\rm nd}$-order.

The absence of notable differences between ZFC and FC magnetization curves at low field (0.01 T) clearly indicates that the antiparallel interactions, which are often observed in these alloys, are sufficiently weak in the present sample (see inset of Fig. 3). This also indicates the absence of Ni-Mn antisite

disorder [30], i.e., the excess Mn atoms occupy exclusively the 4*b* sites.

Isothermal magnetization curves $M_T(H)$ for $Ni_2Mn_{1.4}In_{0.6}$, measured between 270–340 K at 2 K steps in temperature- and field-ascending mode, are shown in Fig. 4 b. Since this compound shows a second order phase transition the magnetic entropy ΔS can be reliably calculated using the Maxwell relations [31]. The entropy change curves are broad and exhibit maxima at 3.3 J/kg K and 6.3 J/kg K for 0–2 and 0–5 T field changes, respectively (see Fig. 4 c). These values are comparable to those observed for Gd [4] within the same temperature range. Finally, in order to fully assess the properties relevant for applications, direct cyclic ΔT_{ad} measurements were performed (for the details, see Supporting Information). We observed $\Delta T_{ad} \approx 1.5$ and ≈ 2 K for $0-1$ T and $0-2$ T field changes, respectively (Fig. 4 d). This demonstrates, that the MCE of a 2^{nd}-order phase transition can be substantially improved, without the use of expensive rare-earth elements. Although lower than Gd, the ΔS and ΔT_{ad} of the present alloy are noticeably higher than those obtained by Moya *et al.* [28] for a very similar composition. Moreover, they are comparable to reversible [32, 8] and even irreversible [33, 34, 35] values observed for some shape memory Heusler alloys at their 1^{st}-order martensitic-austenite transition.

Two central aspects, which make the 2^{nd}-order transition in $Ni_2Mn_{1.4}In_{0.6}$ so attractive for magnetocaloric applications, are the large saturation magnetization of the austenite phase ($M_S = 6.17\ \mu_B$/f.u.) and its proximity to the paramagnetic state at room temperature ($T_C = 316$ K). Noteworthy is the fact that T_C remains almost insensitive to composition, and thus, also to the magnetization, within the whole range of the austenite existence ($0 \leq x \leq 0.4$). This may suggest that it is possible to further improve the properties giving rise to the 2^{nd}-order based room-temperature MCE, i.e. to stabilize the main-group element poor phase in the austenite structure.

The weak variation of T_C with composition x has been clarified by first-principles calculations (see the Supporting Information) based on the experimental lattice parameters of the austenite phase, which were linearly extrapolated to study $x > 0.4$ compositions. We found that the behavior of T_C is almost solely defined by the competition between the positive nearest-neighbor Mn(4*a*/4*b*)–Ni(8*c*) and the negative second-neighbor Mn(4*a*)–Mn(4*b*) contributions scaling up with x, and remains nearly constant because the slower increase of the second contribution is accelerated by the factor x. The detailed plot on Fig. S1 b, shows that the computed maximal eigenvalue of the effective exchange matrix, which corresponds to T_C, stays constant until $x \approx 0.4$. Further increasing x violates the compensation of exchange interactions due to the sudden growth of the diagonal terms resulting from the shortening of the inter-atomic distance.

As we see, the compositional range in which T_C remains constant correlates with the stability range of the austenite phase itself ($x \leq 0.4$). How to stabilize the austenite phase for the Mn-rich compositions? Despite that there is no unique mechanism causing the distortion of the cubic lattice for a particular Heusler composition, most of the Heusler compositions are known to be cubic. This indicates that, by offering a system more degrees of freedom, the

cubic phase may be stabilized, i.e. we may look for more diverse compositions. Regardless the origin of a particular mechanism, in the sense of the electronic structure description, the instability is manifested by the relatively high density of states at the Fermi energy (n_F). As it follows from first-principles calculations (see Supporting Information), n_F grows monotonously with x, but starting from $x \approx 0.4$ this growth substantially accelerates and the most significant contribution to n_F comes from Ni($8c$) states.

Since the exchange coupling mechanisms discussed above are weakly affected by the choice of main-group element, especially within the Mn-rich regime (the phase diagrams of $Ni_2Mn_{1+x}Z_{1-x}$ for Z=In, Sn and Sb look very similar [25]), the reasonable way would be to focus on replacing Ni. By replacing Ni with Co, as in e.g. Ni-Co-Mn-X (X = In, Sn) alloys [36, 37], the austenite phase is stabilized leading to a higher moment, but also a strong increase of T_C. In contrast, replacing Ni by Pd as in e.g. $(Pd_{1-y}Co_y)_2MnSn$ [38] strongly reduces T_C whereas the decrease in M_S is comparatively negligible. Thus, these two mechanisms may be combined by substituting Ni with combination of two different late transition elements, one with a stronger, and another one with a weaker parallel exchange coupling to Mn in $4a/4b$. Good candidates might be the Pd-based $L2_1$ Heusler systems, such as $(Pd_{0.8}Co_{0.2})_2MnSn$ [38], with $T_C = 310$ K and $M_S = 4.43\ \mu_B$/f.u., which is even higher than that of Ni_2MnIn. Here one can expect, that by replacing the ordered Ni sublattice with a randomly occupied (Pd-Co) one, the instability peaks of n_F may be reduced by disorder-induced broadening, and the system may retain the austenite phase for higher Mn-In substitution ratios. In addition, since the T_C of $(Pd_{1-y}Co_y)_2MnSn$ compositions strongly depends on the balance between Pd and Co [38], we obtain one extra degree of freedom, which can be efficiently used to fine tune T_C to the desired working temperatures for applications.

In summary we have analyzed the Heusler class of materials looking for systems presenting large ground state moments which can be stabilized into a fully austenite state with a 2^{nd}-order phase transition around room temperature. We have pinpointed a composition - $Ni_2Mn_{1.4}In_{0.6}$ - which has been experimentally studied and shown to present the desired magneocaloric properties. Based on additional first-principles calculations we explain the underlying mechanisms and point out a perspective for further improvement. Thus our study consists of a set of rules - and a proof of concept - for finding Heusler alloys showing large ground state magnetic moment and reversible MCE aiming at applications.

Acknowledgements

The authors would like to thank Dr. Franca Albertini from IMEM-CNR, Parma-Italy, for useful discussions. This work was financially supported by the Deutsche Forschungsgemeinschaft DFG (Project No. TP 1.2-A of Research Unit FOR 1464 ASPIMATT) and by the ERC Advanced Grant (No. 291472) Idea Heusler. S. S. thanks Alexander von Humboldt for fellowship.

References

[1] V. K. Pecharsky, K. A. Gschneidner, Jr., *Phys. Rev. Lett.* **1997**, *78*, 4494.

[2] M. Annaorazov, K. Asatryan, G. Myalikgulyev, S. Nikitin, A. Tishin, A. Tyurin, *Cryogenics* **1992**, *32*, 867.

[3] H. Wada, Y. Tanabe, *Appl. Phys. Lett.* **2001**, *79*, 3302.

[4] O. Tegus, E. Brück, K. H. J. Buschow, F. R. de Boer, *Nature* **2002**, *415*, 150.

[5] N. H. Dung, Z. Q. Ou, L. Caron, L. Zhang, D. T. C. Thanh, G. A. de Wijs, R. A. de Groot, K. H. J. Buschow, E. Brück, *Adv. Energy Mater.* **2011**, *1*, 1215.

[6] F. Hu, B. Shen, J. Sun, , G. Wu, *Phys. Rev. B* **2001**, *64*, 132412.

[7] T. Krenke, M. Acet, E. F. Wasermann, X. Moya, L. Mañosa, A. Planes, *Nature Mater.* **2005**, *4*, 450.

[8] J. Liu, T. Gottschal, K. P. Skokov, J. D.Moore, O. Gutfleisch, *Nature Materials* **2012**, *11*, 620.

[9] L. Pareti, M. Solzi, F. Albertini, A. Paoluzi, *Eur. Phys. J. B* **2003**, *32*, 303.

[10] J. Torrens-Serra, C. Biffi, R. Santamarta, V. Recarte, J. Pérez-Landazábal, A. Tuisi, E. Cesari, *Materials Characterization* **2014**, *93*, 24.

[11] G. V. Brown, *J. Appl. Phys.* **1976**, *46*, 3673.

[12] A. M. Tishin, Y. I. Spichkin, *The Magnetocaloric Effect and its Applications*, Institute of Physics Publishing: Bristol, **2003**.

[13] B. Yu, M. Liu, P. W. Egolf, A. Kitanovski, *Int. J.Refrig.* **2010**, *33*, 1029.

[14] S. Singh, S. E. Muthu, A. Senyshyn, P. Rajput, E. Suard, S. Arumugam, S. R. Barman, *Appl. Phys. Lett.* **2014**, *104*, 051905.

[15] S. Singh, S. W. D'Souza, K. Mukherjee, P. Kushwaha, S. R. Barman, S. Agarwal, P. K. Mukhopadhyay, A. Chakrabarti, E. V. Sampathkumaran, *Appl. Phys. Lett.* **2014**, *104*, 231909.

[16] S. Fuji, S. Sugimura, S. Ishida, S. Asano, *J. Phys.: Cond. Mat.* **1990**, *2*, 8583.

[17] P. J. Brown, K.-U. Normann, P. J. Webster, K. R. A. Ziebeck, *J. Phys.: Cond. Mat.* **2000**, *12*, 1827.

[18] G. H. Fecher, H. C. Kandpal, S. Wurmehl, C. Felser, *J. Appl. Phys.* **2006**, *99*, 08J106.

[19] J. Kübler, G. H. Fecher, C. Felser, *Phys. Rev. B* **2007**, *76*, 024414.

[20] S. Wurmehl, G. H. Fecher, H. C. Kandpal, V. Ksenofontov, C. Felser, H.-J. Lin, *Phys. Rev. B* **2005**, *72*, 184434.

[21] S. Wurmehl, G. H. Fecher, H. C. Kandpal, V. Ksenofontov, C. Felser, H.-J. Lin, *Appl. Phys. Lett.* **2006**, *88*, 032503.

[22] B. Balke, G. H. Fecher, H. C. Kandpal, C. Felser, K. Kobayashi, E. Ikenaga, J.-J. Kim, S. Ueda, *Phys. Rev. B* **2006**, *74*, 104405.

[23] M. Jourdan, J. Minár, J. Braun, A. Kronenberg, S. Chadov, B. Balke, A. Gloskovskii, M. Kolbe, H. J. Elmers, G. Schönhense, H. Ebert, C. Felser, M. Kläui, *Nature Comm.* **2014**, *5*, 3974.

[24] S. Chadov, S. W. D'Souza, L. Wollmann, J. Kiss, G. H. Fecher, C. Felser, *Phys. Rev B* **2015**, *91*, 094203.

[25] Y. Sutou, Y. Imano, N. Koeda, T. Omori, R. Kainuma, K. Ishida, K. Oikawa, *Appl. Phys. Lett.* **2004**, *85*, 4358.

[26] T. Kanomata, T. Yasuda, S. Sasaki, H. Nishihara, R. Kainuma, W. Ito, K. Oikawa, K. Ishida, K.-U. Neumann, K. R. A. Ziebeck, *J. Magn. Magn. Mat.* **2009**, *321*, 773.

[27] T. Krenke, M. Acet, E. F. Wassermann, X. Moya, L. Mañosa, A. Planes, *Phys. Rev. B* **2006**, *73*, 174413.

[28] X. Moya, L. Mañosa, A. Planes, S. Aksoy, M. Acet, E. F. Wasermann, T. Krenke, *Phys. Rev. B* **2007**, *75*, 184412.

[29] A. K. Nayak, C. S. Mejia, S. W. D'Souza, S. Chadov, Y. Skourski, C. Felser, M. Nicklas, *Phys. Rev. B* **2014**, *90*, 220408(R).

[30] S. Singh, R. Rawat, S. E. Muthu, S. W. D'Souza, E. Suard, A. Senyshyn, S. Banik, P. Rajput, S. Bharadwaj, A. M. Awasthi, R. Ranjan, S. Arumugam, D. Schlagel, T. Lograso, A. Chakrabarti, S. R. Barman, *Phys. Rev. Lett.* **2012**, *109*, 246601.

[31] L. Caron, Z. Q. Ou, T. T. Nguyen, D. T. C. Thanh, O. Tegus, E. Brück, *Journal of Magnetism and Magnetic Materials* **2009**, *321*(21), 3559–3566.

[32] T. Gottschall, K. P. Skokov, B. Frincu, O. Gutfleisch, *Applied Physics Letters* **2015**, *106*(2), 021901.

[33] V. V. Khovaylo, K. P. Skokov, Y. S. Koshkid'ko, V. V. Koledov, V. G. Shavrov, V. D. Buchelnikov, S. V. Taskaev, H. Miki, T. Takagi, A. N. Vasiliev, *Phys. Rev. B* **2008**, *78*, 060403 (R).

[34] M. Pasquale, C. P. Saso, L. H. Lewis, L. Giudici, T. Lograso, D. Schlagel, *Phys. Rev. B* **2005**, *72*, 094435.

[35] I. Titov, M. Acet, M. Farle, D. Gonzalez-Alonso, A. P. L. Manosa, T. Krenke, *J. Appl. Phys.* **2012**, *112*, 073914.

[36] D. Cong, S. Roth, L. Schultz, *Acta Materialia* **2012**, *60*(13–14), 5335 – 5351.

[37] R. Kainuma, K. Ito, W. Ito, R. Umetsu, T. Kanomata, K. Ishida, *Materials Science Forum* **2009**, *635*, 23–31.

[38] E. Uhl, *Solid State Communications* **1985**, *53*(4), 395 – 398.

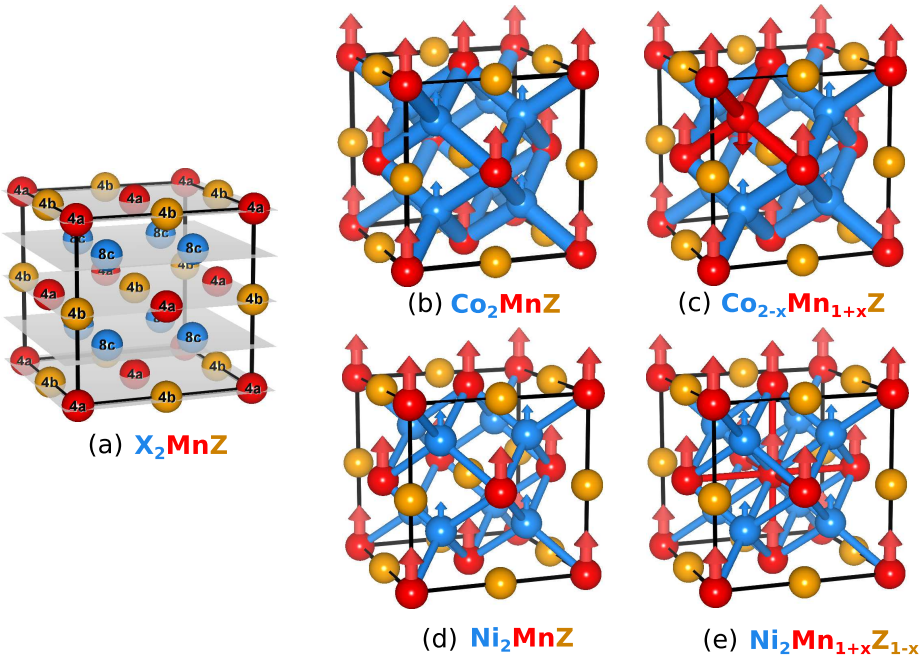

Figure 1: **The effects of different chemical substituions on the magnetic structure of the austenite phase.** (a) Unit cell of the $L2_1$ structure (Wyckoff sites $4a$, $4b$ and $8c$ are marked by red, yellow and blue colors, respectively) corresponding to the $X_2\mathrm{Mn}Z$ (X - late transition element, Z - main group element) composition. The color of a particular Wyckoff site matches that of the occupying element. (b) $L2_1$ structure with $\mathrm{Co_2Mn}Z$ composition, for simplicity only magnetic sublattices (Mn in $4a$ and Co in $8c$) are shown. Local magnetic moments are marked by arrows. Nearest Co($8c$) and Mn($4a$) neighbor moments are strongly coupled by the parallel exchange interaction shown as thick blue bonds. (c) This picture distorts for $\mathrm{Co}_{2-x}\mathrm{Mn}_{1+x}\mathrm{Si}$ compositions: extra Mn substitutes Co in $8c$ and couples antiparallel (red bonds) to the Mn in $4a$. (d) In case of $\mathrm{Ni_2Mn}Z$, the parallel Mn-Ni coupling is much weaker compared to (b) (thin blue bonds). (e) In case of $\mathrm{Ni_2Mn}_{1+x}Z_{1-x}$, excess Mn randomly substitutes Z atoms in the $4b$ sites (indicated by mixed-colored spheres). This leads to the emergence of antiparallel Mn($4a$)–Mn($4b$) exchange coupling (indicated by the red bonds).

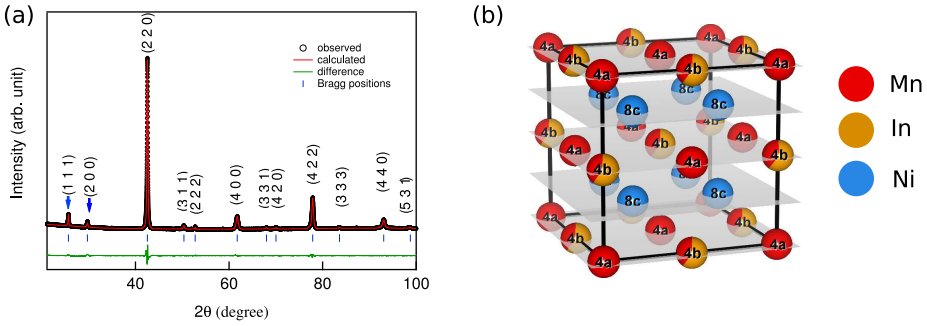

Figure 2: **Structural analysis of the $Ni_2Mn_{1.4}In_{0.6}$ sample.** (a) Room-temperature XRD pattern of $Ni_2Mn_{1.4}In_{0.6}$. Observed, calculated and residual patterns are marked by the black dots, red solid line and green solid line, respectively. Blue ticks indicate the Bragg peaks positions, blue arrows – the superstructure reflections of the $L2_1$ phase. (b) The unit cell of $Ni_2Mn_{1.4}In_{0.6}$ as deduced from XRD: $4a$ Wyckoff sites are occupied by Mn (red), $4b$ - are randomly occupied by Mn and In (red/yellow), $8c$ - by Ni (blue).

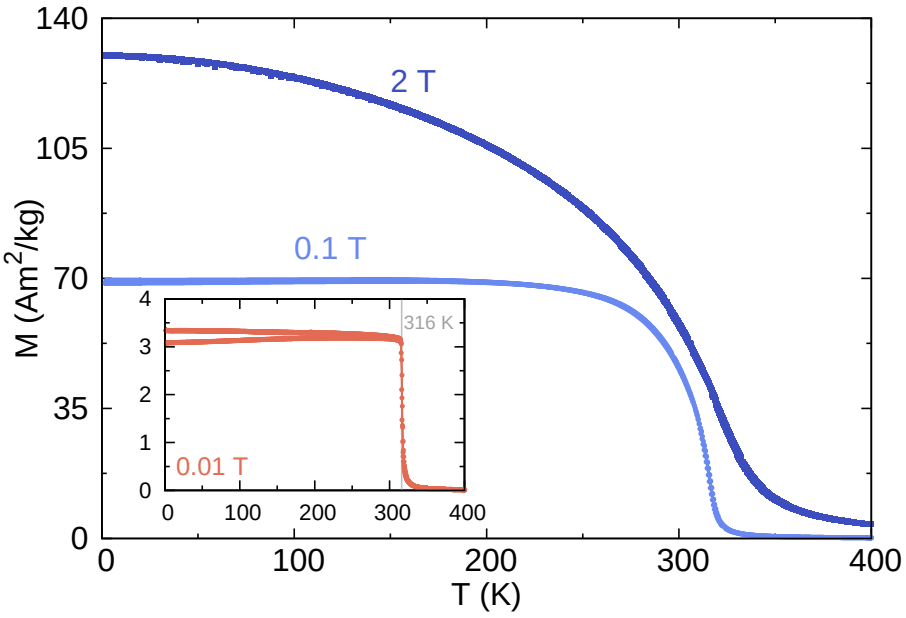

Figure 3: **Magnetic properties of $Ni_2Mn_{1.4}In_{0.6}$ sample.** Zero-field-cooled heating (ZFC), field-cooling (FCC) an field heating (FCH) magnetization curves of $Ni_2Mn_{1.4}In_{0.6}$ in different magnetic fields. The inset shows the magnetization measured in a weak magnetic field of 0.01 T. The $T_C \approx 316$ K is indicated by a vertical line.

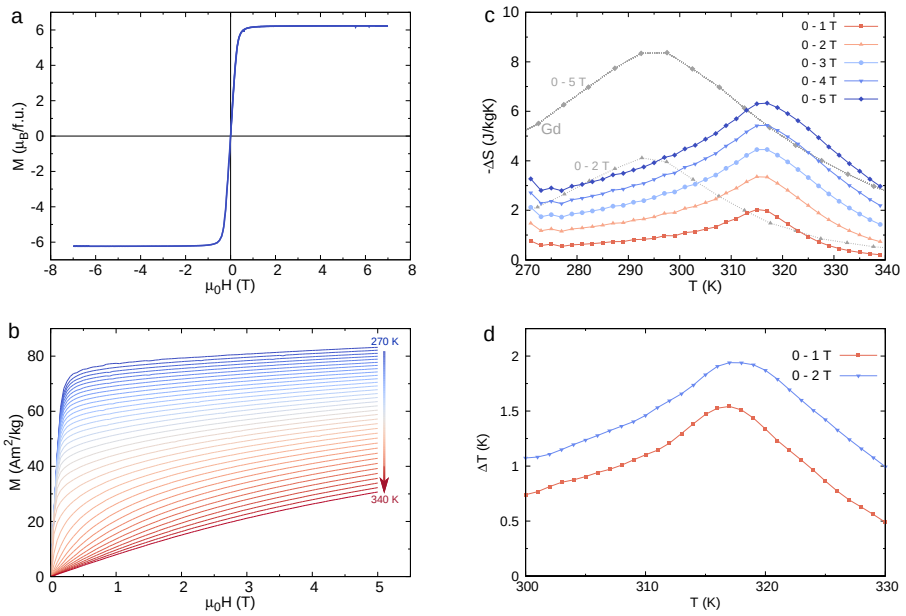

Figure 4: **MCE properties of $Ni_2Mn_{1.4}In_{0.6}$ sample** (a) The isothermal magnetization curve at 2 K. (b) Isothermal magnetization measured between 270 K $< T <$ 340 K at 2 K steps. (c) Magnetic entropy change ΔS as a function of temperature for different field changes; the ΔS of $Ni_2Mn_{1.4}In_{0.6}$ is compared to that of Gd (after Tegus *et al.* [4]). (d) Adiabatic temperature change ΔT_a measured as a function of temperature for two magnetic field changes.